Ocean Engineering 269 (2023) 113574

Contents lists available at ScienceDirect

Ocean Engineering

journal homepage: www.elsevier.com/locate/oceaneng

Strouhal number for boundary shear flow past a circular cylinder in the subcritical flow regime

Yan Liu [a,b], Jun Liu [a,b], Fu-Ping Gao [a,b,*]

[a] Institute of Mechanics, Chinese Academy of Sciences, Beijing, 100190, China
[b] School of Engineering Science, University of Chinese Academy of Sciences, Beijing, 100049, China

ARTICLE INFO

Handling Editor: Prof. A.I. Incecik

Keywords:
Vortex shedding
Bed-proximity effects
Shear flow
Particle image velocimetry (PIV)
Circular cylinder

ABSTRACT

Strouhal number (*St*) is an essential dimensionless quantity for characterizing the vortex-shedding frequency of the flow past a cylinder. In this study, the Strouhal number for a near-wall circular cylinder fully immersed in a boundary shear flow in the subcritical flow regime was experimentally investigated in a water flume. The velocity fluctuations and flow fields of the lee-wake were systematically measured with an Acoustic Doppler Velocimeter (ADV) and an upward-illumination Particle Image Velocimetry (PIV) system, respectively. Based on dimensional analyses, a non-dimensional shear parameter (*K*) is introduced to characterize the shear flow. An explicit expression between *K* and *e/D* is obtained on the basis of the boundary theory and verified with the flume measurements. Spectral analysis of wake velocities indicates that the multi-peaks can be identified as the cylinder gets closer to the wall. The PIV measurements indicate that the multi-peaks spectra are predominantly induced by the intense interactions between the lower shear layer and wall boundary layer. By fitting the experimental results, empirical relationships for the variations of *St* with *K* or *e/D* are finally established for the subcritical flow regime.

1. Introduction

When the flow is passing a circular cylinder under wall-free conditions, alternate and periodic shedding of Kármán vortices would be formed in the wake. Nevertheless, as the cylinder is approaching the bed, i.e., under near-wall conditions, the lee-wake dynamics would be significantly altered in the boundary layer flow (see Lei et al., 1999; Sumer, 2006; Gao, 2017). Significant consequences could be generated by such lee-wake dynamics in offshore engineering practices, e.g., the local scour (see Fredsøe et al., 1987; Gao et al., 2006), the on-bottom stability (see Gao et al., 2003; Fredsøe, 2016) and the vortex-induced vibrations of submarine pipelines (see Blevins, 1990; Yang et al., 2008; Wang et al., 2013).

The lee-wake dynamics behind a near-wall cylinder in the shear flow involve an asymmetric vortex-shedding, the deviation of separation points and the appearance of a series of wall vortices (see Fig. 1). The positive vorticity of the lower shear layer can be weakened by negative vorticity in the wall boundary layer when the cylinder approaches the bed; meanwhile, the wall vortices would interact with the von-Kármán vortices shed from the lower shear layer. If the vorticity strength of the lower shear layer is not enough to roll up to form vortices, the regular Kármán-like vortex-shedding can thereby be suppressed below a critical gap ratio e/D ($\approx$0.30), where e is the gap between the cylinder bottom and the bed, and D is the outer diameter of the cylinder (see Fig. 1) (Bearman and Zdravkovich, 1978; Lei et al., 2000; Price et al., 2002; Wang and Tan, 2008). Note that the flow separation mechanism for bluff bodies with different geometry shapes could be different. For example, the flow regime for the smooth circular cylinder mainly depends on the Reynolds number (Lienhard, 1966; Dash and Lee, 2014), while that for a trapezoidal cylinder was also affected by the cylinder's shape, size, and orientation. Based on the location of the flow separation point on the trapezoidal cylinder, Bhunia et al. (2019) ever classified the wake flow regime into three types; while four different flow regimes for a square cylinder with two splitter plates have been identified from the observations of Dash et al. (2020).

Strouhal number (*St*) is an essential dimensionless quantity for characterizing the vortex-shedding frequency (f_s) of the flow passing a cylinder. The vortex-shedding frequency obeys the Strouhal law, i.e., $St = f_s D/u_c$, in which u_c is the approach velocity at the center height of the cylinder (Zdravkovich, 1997). Under the wall-free condition, *St* is predominantly related to the Reynolds number (Sarpkaya, 2010). Herein, the Reynolds number is defined as $Re = u_c D/\nu$, where ν is the kinematic

* Corresponding author. Institute of Mechanics, Chinese Academy of Sciences, Beijing, 100190, China.
E-mail address: fpgao@imech.ac.cn (F.-P. Gao).

https://doi.org/10.1016/j.oceaneng.2022.113574
Received 9 June 2022; Received in revised form 11 December 2022; Accepted 26 December 2022
Available online 29 December 2022

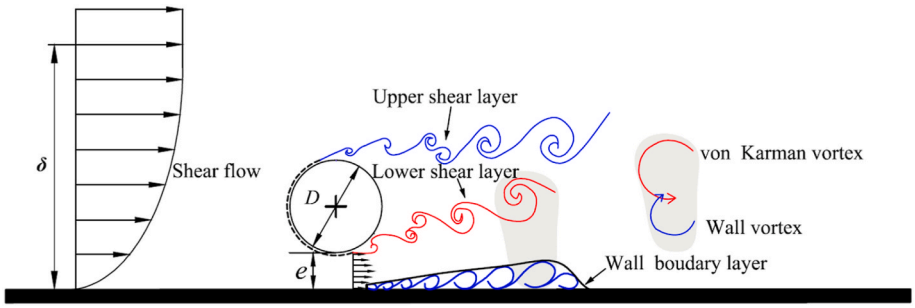

Fig. 1. Illustration for the vortex shedding of a near-wall cylinder in the shear flow: the vortex line -(solid lines in red) indicates positive vorticity; -(solid lines in blue) indicates negative vorticity. (For interpretation of the references to colour in this figure legend, the reader is referred to the Web version of this article.)

viscosity of water ($\nu \approx 1.004 \times 10^{-6}$ m^2/s at 20 °C). As reported by Sarpkaya (2010), the value of *St* is around 0.2 for smooth cylinders at the subcritical Reynolds numbers, i.e., $300 < Re < 3.0 \times 10^5$. In such a subcritical flow regime, the boundary layer along the surface of an isolated circular cylinder is laminar, while the wake outside is completely turbulent (Niemann and Holscher, 1990). Nevertheless, as stated above, the flow characteristics behind the cylinder could be significantly influenced when the circular cylinder gets close to the bed, which may further have certain effects on the vortex-shedding frequency.

In the past few decades, the vortex-shedding from a cylinder in the shear flow has drawn much attention among researchers. Previous experiments regarding the shear effects on the wake at the rear of a wall-free cylinder were predominantly carried out under linear (or uniform) shear flow conditions. In the water tank tests by Kiya et al. (1980), the linear shear flows were generated by a honeycomb-shaped guidance device installed upstream of the test section; the flow was visualized with hydrogen bubbles or the electrolytic-dye production, and a hot-film sensor was used to detect the velocity fluctuations in the wake of the cylinder in moderate-Reynolds-number shear flows (Re = 35–1500). Their observations indicated that the critical Reynolds number beyond which the vortex-shedding occurs in a shear flow was higher than that in a uniform flow and increased approximately linearly with the shear parameter (K) for $K > 0.06$, where $K = GD/u_c$, in which G is the transverse velocity gradient of the shear flow. Test results of the recirculating water tunnel experiment by Kwon et al. (1992) indicated that the values of *St* increased nonlinearly with increasing *Re* when $Re < 400$ and reached a nearly-constant value ($St \approx 0.22$) when $Re \geq 400$–700 for a fixed value of K in the range of $0 \leq K \leq 0.25$; moreover, for relatively higher values of K (e.g., $K = 0.19$–0.25), the value of *St* was appreciably higher than that in a uniform flow ($K = 0$). By employing a low-speed, closed-return wind tunnel, Sumner and Akosile (2003) investigated the shear effects on the vortex shedding behind the circular cylinder in the sub-critical flow regime (the examined *Re* ranged from 4.0×10^4 to 9.0×10^4). Their measurements showed that the low to moderate shear parameter (K = 0.02–0.07) did not appreciably influence the Strouhal number, although it had been commonly recognized that the Strouhal number generally increases as the shear parameter K increases (see Kiya et al.,1980; Kwon et al., 1992). Similarly, the wind tunnel test results by Cao et al. (2007) indicated that the Strouhal number was almost unchanged when $K < 0.27$ at the sub-critical Reynolds number.

Besides the aforementioned studies regarding the Strouhal number for the cylinder immersed in a uniform or linear shear flow (without bed-boundary), the bed-proximity effects on vortex shedding from a cylinder in the boundary shear flow have also been investigated. A wind tunnel of the closed-return type was employed by Bearman and Zdravkovich (1978) to investigate the effects of e/D on the vortex-shedding of a near-wall cylinder at $Re = 2.5 \times 10^4$ and 4.8×10^4. In their experiments, a thin plate was introduced into the flow to represent the wall, so that only the thin turbulent boundary layer was taken into account, the thickness of which was found to be about 1.5 cm (0.8 D). Spectral analysis of hot-wire signals demonstrated that regular vortex shedding was suppressed for $e/D < 0.30$, i.e., the peak frequency in all spectra for $e/D < 0.30$ was either absent or at least an order of magnitude weaker than that for $e/D > 0.30$; moreover, the Strouhal number was remarkably constant for $e/D > 0.30$. As observed later by Angrilli et al. (1982) with an open water channel for the examined three values of Re (= 2860, 3820, and 7640), the proximity of the bed induced a slight increase of vortex-shedding frequency up to 1.11 times of that for the wall-free cylinder ($f_{\text{wall-free}}$), i.e., $f_s/f_{\text{wall-free}} \approx 1.11$ when e/D was decreased to 0.5. Similar observations were made by Grass et al. (1984) for the two cases of shear and uniform approach flows, indicating the Strouhal number progressively increased as the values of e/D decreasing below 2.0, which was regarded to be attributed to large velocity gradients and bed proximity. By employing a wind tunnel, Lei et al. (1999) investigated the vortex shedding of a circular cylinder immersed in different boundary layers at Reynolds numbers from 1.30×10^4 to 1.45×10^4. Their results showed that the Strouhal number increases with the increase of the non-dimensional velocity gradient, which is comparable with the test results of Kiya et al. (1980). Price et al. (2002) further observed the vortex-shedding over a cylinder in a boundary layer flow ($1200 < Re < 4960$) by using the flow visualization with Rhodamine and Fluorescein dyes, Particle Image Velocimetry (PIV) and hot-film anemometry. They found that, for $Re < 2.6 \times 10^3$, the Strouhal number for $e/D < 2.0$ is greater than that for an isolated wall-free circular cylinder; while *St* seemed to be insensitive to e/D for $Re \geq 4.0 \times 10^3$. Their results were later confirmed by the observations in a recirculating water channel by Lin et al. (2009). Lin et al. (2009) reported that the regular and alternate vortex shedding was suppressed as the cylinder approached the bed (also see Lei et al., 2000); however, the dominant frequency was still detected in the wake, which can further induce the vibration of the near-wall cylinder (Liu and Gao, 2022). For $Re < 2.2 \times 10^3$, there exists a gap ratio at which the power spectra exhibit multi-peak or broadband characteristics, which was deemed as the result of the random switching of gap flow (Lin et al., 2009). Similarly, Wang and Tan (2008) investigated the flow characteristics in the near wake of a circular cylinder located close to a fully developed turbulent boundary layer by using PIV. Their results showed that the Strouhal number is insensitive to e/D and roughly keeps constant at about 0.19 over the range of $0.20 \leq e/D \leq 1.0$ at $Re = 1.2 \times 10^4$ and the incident boundary layer thickness (δ) was about 0.4D. Unlike the results of Wang and Tan (2008), the observations by Zhou et al. (2021) indicated that the Strouhal number is dependent on the gap ratio e/D, and the *St* increases as the gap ratio decreases down to $e/D = 0.25$ at the examined $Re = 1.5 \times 10^3$ and $\delta = 0.65D$. Note that in most of the aforementioned investigations on the bed-proximity effect, the shear parameter (K) was not provided for the boundary shear flow.

In a summary of the previous studies, the effects of gap ratio (e/D) and shear parameter (K) on the vortex-shedding frequency of a near-wall cylinder were generally regarded as two independent influential factors. There still exist certain discrepancies regarding the variation trends for *St* under the bed-proximity condition. The variations of *St* with both e/D

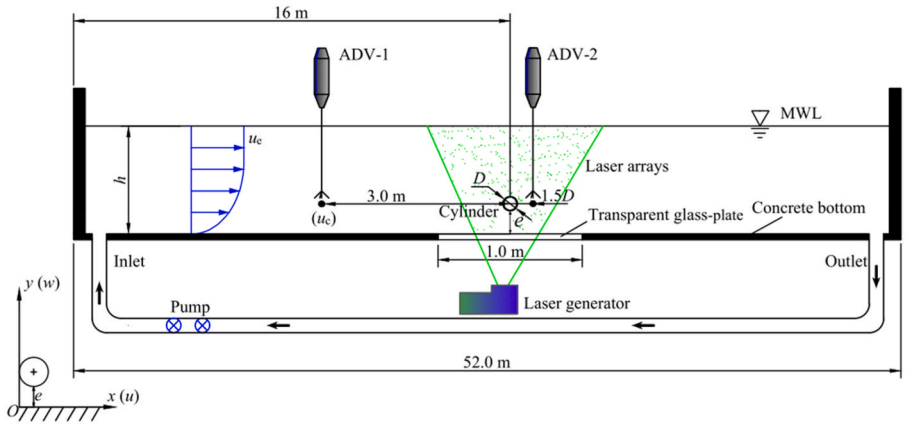

(a)

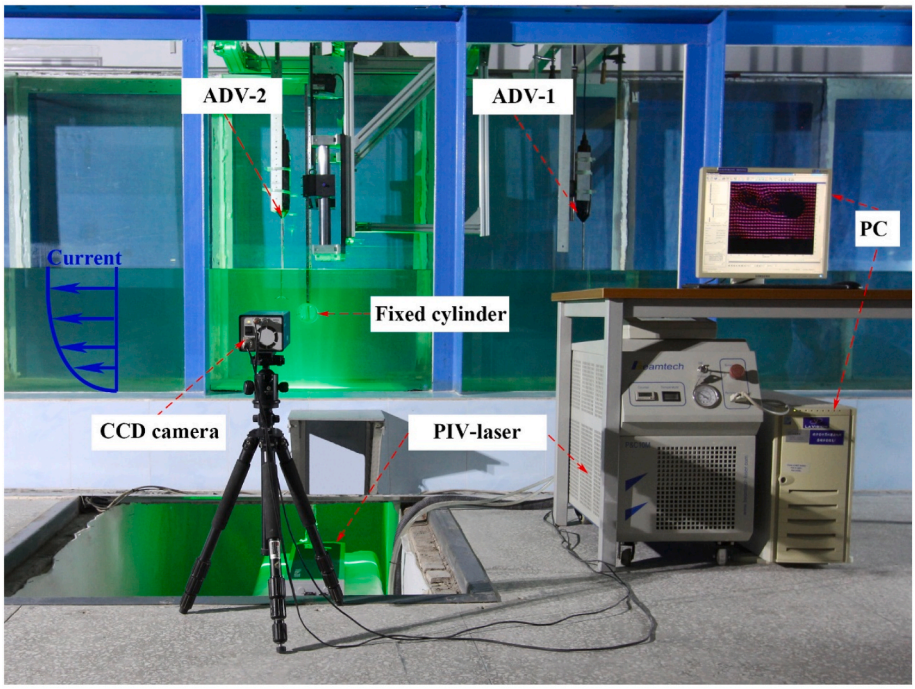

(b)

Fig. 2. (a) Schematic diagram of the water flume; (b) Snapshot picture of the test section (viewed from the opposite direction as depicted in Fig. 2(a)).

and K have not been well understood.

In the present study, a series of flume experiments were conducted to re-examine the bed-proximity effects on the Strouhal number for a circular cylinder fully immersed in a boundary shear flow in the subcritical flow regime. The correlation of the gap ratio with the shear parameter is made on the basis of the boundary layer theory. The vortex-shedding frequency was measured with ADV and interpreted with power spectral analysis; meanwhile, flow visualization was conducted with a specially arranged PIV system. By fitting the experimental results, the empirical relationships between St and K or e/D were finally established.

2. Methodology and experimental setup

2.1. Dimensional analyses on the vortex shedding frequency of a near-wall cylinder

As illustrated in Fig. 1, vortex shedding is one of the typical characteristics in the wake of the near-wall cylinder, which involves complex interactions between the circular cylinder, the plane bed, and the shear flow. The vortex shedding frequency of the near-wall cylinder (f_s) is mainly related to the following parameters:

$$f_s = \xi_1(\rho, \nu, u_c, D, e, \delta, ...) \tag{1}$$

where ρ is the mass density of water ($\rho \approx 1.0 \times 10^3$ kg/m^3 at 20 °C); δ is the thickness of the free-stream boundary layer.

According to Prandtl's boundary layer theory, the velocity profile of the turbulent boundary layer along a smooth wall can be approximately expressed as a power law:

$$u = u_e\left(\frac{y}{\delta}\right)^n \tag{2}$$

which was deemed to be valid for $Re < 10^6$ (see Schlichting, 1979). In Eq. (2), u is the streamwise velocity along with water depth; u_e is the velocity at the water surface; y is the position in the transverse coordinate axis (note: $y = 0$ is on the plane bed, see Fig. 2); n is an empirical parameter related to the Reynolds number of the approach flow, whose values were suggested in the range of 1/10–1/6 (Schlichting, 1979). In the present study, the value of n is set as 1/7. It should be mentioned that

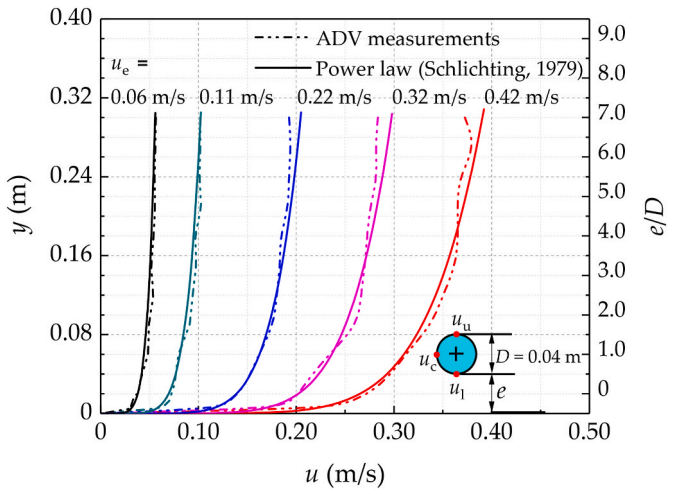

Fig. 3. Flume measurements and the corresponding predictions of the vertical velocity profiles at the test section for five typical flow velocities.

the velocity distribution of power law (Eq. (2)) ignores the thin viscous sublayer. The logarithmic law was previously employed for describing the velocity profiles under turbulent flow conditions (e.g., Adrian et al. (2000); Wang and Tan (2008); Liu and Gao (2022)). By performing the derivative of u with respect to y in Eq. (2), the transverse velocity gradient (G) can be derived as

$$G = \frac{nu_e}{\delta}\left(\frac{y}{\delta}\right)^{n-1} \tag{3}$$

It is indicated that the velocity gradient (G) at the level of the cylinder's center ($y = e + 0.5D$) can be calculated once the values of δ and u_e are provided. That is, if the values of D, δ and u_e are given, the parameter e in Eq. (1) can be replaced with G. Based on Buckingham's Π theorem with choosing u_c, ν, and D in Eq. (1) as the three independent parameters, the Strouhal number (St) for the boundary shear flow past a circular cylinder can be determined by an assembly of dimensionless parameters:

$$St = \xi_2\left(Re, K, \frac{\delta}{e+D}, \ldots.\right) \tag{4}$$

where K ($= GD/u_c$) is the shear parameter of a shear flow; and $\delta/(e + D)$ is the ratio of the boundary layer thickness (δ) to the distance from the cylinder's top to the bed surface ($e + D$). For $\delta/(e + D) > 1.0$, the cylinder is fully immersed in the boundary layer.

2.2. Experimental set-up

The experiments were performed in a large water flume (52.0 m long, 1.0 m wide, 1.5 m high) located at the Institute of Mechanics, Chinese Academy of Sciences. The water depth (h) was maintained at 0.50 m during all the flume tests. Fig. 2(a) gives the schematic diagram of the water flume. The test section (see Fig. 2(b)) was located at a distance of 16.0 m from the inlet of the flume. The test cylinder with varied gap ratios was mounted horizontally in the symmetry plane of the test section. The origin of the Cartesian coordinate system is set at the intersection between the cylinder's leading edge and the bed. The coordinates x and y denote the streamwise and the vertical directions, respectively (see Fig. 2(a)).

On the upstream side with a distance of 3.0 m apart from the cylinder, an Acoustic Doppler Velocimeter (labeled "ADV-1") was used to measure the approach velocity (far-field) at the height of the cylinder center (u_c) with a sampling rate of 100 Hz. Meanwhile, another ADV (labeled "ADV-2") was used to measure the wake velocity fluctuation with the same sampling rate (100 Hz). ADV-2 was located at the height

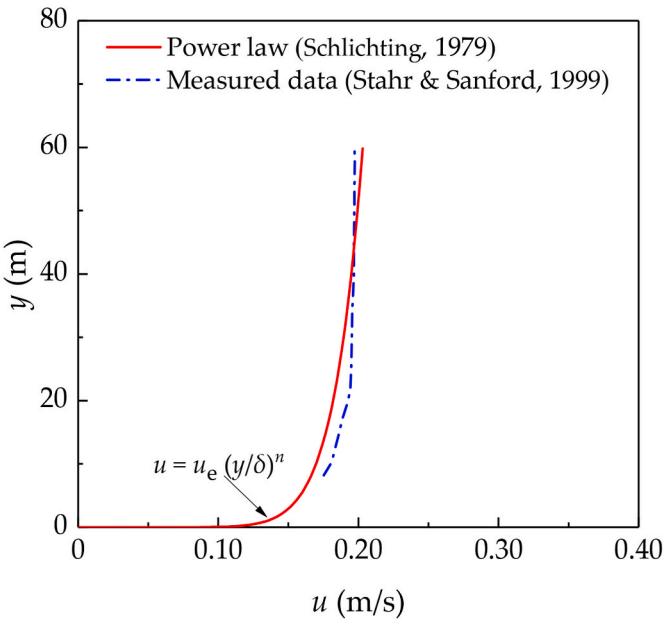

Fig. 4. The measured and the predicted profiles for the transverse velocity of the shear flow over the Blake Outer Ridge in the North Atlantic Western Boundary Current (Stahr and Sanford, 1999).

of the cylinder center on the downstream side with a distance of 1.5D apart from the cylinder. Both the far-field and the lee-wake velocities were recorded synchronously. As shown in Fig. 2(b), the flow visualization was performed by employing a PIV system, which includes an impulse laser, a CCD (Charge Coupled Device) camera and a PC (Personal Computer), etc. The flow field around the cylinder was illuminated by the laser sheet and then captured by the CCD camera. The data of the flow field were then acquired and post-processed by the PC, and the evolution of the wake flow field around the cylinder in the x-O-y plane was finally obtained. More details on the PIV system will be further discussed in Section 2.2.2.

2.2.1. Flow conditions

The vertical distribution of the streamwise velocity u in the fully developed approach shear flow was firstly measured by an ADV at various levels (y) along the water depth at the test section in the absence of the cylinder. Fig. 3 depicts the profiles of the mean streamwise velocity for five values of flow velocity. The predictions with the empirical power law (i.e., Eq. (2)) are also provided in this figure. It is indicated that the measured velocity profiles agree well with the predictions.

As shown in Fig. 3, the boundary layers extend up to the free surface in the present flume tests. Thus, the boundary layer thickness can be regarded to be equal to the water depth, i.e., $\delta \approx h$. The displacement thickness of the boundary layer can be calculated with $\delta_d = \int_0^\delta (1 - u(y)/u_c)\mathrm{d}y$, i.e., $\delta_d \approx 6.3$ cm; and the corresponding momentum thickness can be calculated with $\delta_m = \int_0^\delta \frac{u(y)}{u_c}(1 - u(y)/u_c)\mathrm{d}y$, i.e., $\delta_m \approx 4.9$ cm. The shape factor H_{dm} ($= \delta_d/\delta_m$) ≈ 1.3, indicating that the turbulent boundary layer was fully developed (see Adrian et al., 2000). For all the examined gap ratios ($0.10 \le e/D \le 2.0$, see Fig. 3), the test cylinder was fully immersed in the turbulent boundary layer.

As a typical near-wall cylinder, submarine pipeline is vulnerable to the shear flow along the seabed. As shown in Fig. 4, the deep-ocean velocity profile in the North Atlantic Western Boundary Current over the Blake Outer Ridge was measured by Stahr and Sanford (1999) with the Absolute Velocity Profiler (AVP). For comparisons, the velocity profile predicted by the power law is also presented in Fig. 4, which is generally consistent with the field measurements. The benthic boundary layer (BBL) is usually thin (O (10 m)) in comparison with the ocean

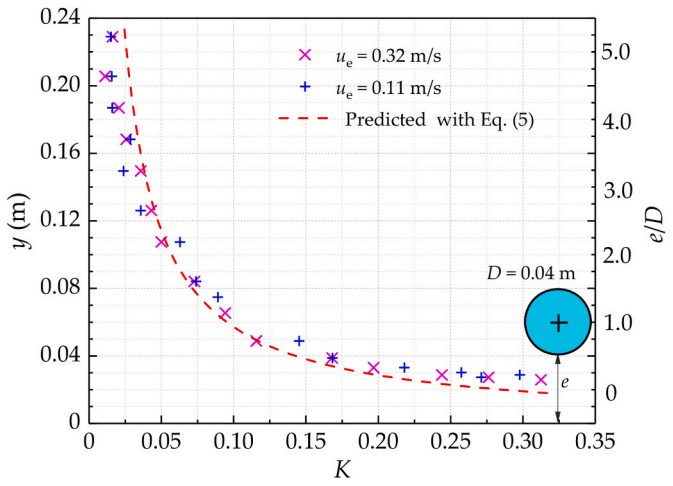

Fig. 5. The shear parameter distribution across the test section.

depths of ~4000 m (Lueck et al., 2009). The thickness of BBL is generally up to ten times thicker than the diameter of submarine pipeline (O (1 m)). As such, submarine pipelines in the field are fully immersed in the benthic boundary layer, which is under the same condition as the present flume tests (see Fig. 3).

As for the shear parameter K (i.e., $K = GD/u_c$), the values of u_c and G in a boundary shear flow can be evaluated with Eqs. (2) and (3), respectively. Note that, $u_c = u|_{y=e+0.5\,D}$ and $\delta \approx h$. An explicit expression for the relationship between K and e/D can then be obtained as

$$K = \frac{1}{7.0(0.50 + e/D)} \tag{5}$$

Eq. (5) indicates that the shear parameter (K) is correlated with the gap ratio (e/D) for a boundary layer flow. In the flume tests, the velocity gradient can also be estimated as $G \approx (u_u - u_l)/D$, where u_u is the approach velocity at the level of the upper surface of the cylinder, and u_l is the approach velocity at the level of the cylinder's bottom (see Fig. 3). Thus, the values of K can be calculated with $K \approx (u_u - u_l)/u_c$. The variations of K with e/D for the two selected velocities u_e = 0.11 m/s, and 0.32 m/s are shown in Fig. 5. Theoretical predictions with Eq. (5) are also plotted for comparisons. Satisfactory agreements are found between the experimental results and theoretical predictions.

2.2.2. PIV system and vortex identification methods

An upward-illumination LaVision PIV system was employed to visualize the lee-wake of the near-wall cylinder (see Fig. 2(a)). At the test section of the flume, a transparent glass-plate bottom (1.0 m × 1.0 m) was constructed, through which the 1-mm-thick double-pulsed laser arrays with a wavelength of 532 nm were upwardly illuminating the flow field (see Fig. 2(b)). The water was seeded with silver-coated hollow spherical glass particles and silt particles with good flow-following ability. Such an upward-illumination alignment of the laser sheet can efficiently avoid the impact of laser reflection from the water surface.

A CCD camera with a resolution of 1376 × 1040 pixels was installed outside the flume to capture the images. For a better compromise between the observed area and the accuracy of lee-wake structures, the observation window of the PIV was chosen as 320 mm × 240 mm (i.e., 8.0D × 6.0D for the cylinder diameter D = 0.04 m) in the x-O-y plane, yielding the image with a resolution of about 230 μm/pixel. The displacement vectors were obtained by LaVision Inc.'s DaVis 7.2 software (LaVision Gmbh, 2009) using the cross-correlation algorithm. During the image processing, a rectangle effective interrogation window of 32 × 32 pixels was first used and then stepped down to the window size of 16 × 16 pixels with an overlapping of 50%. Such interrogation and evaluation procedure would yield approximately 5590 (86 × 65) velocity vectors (u, w) with a vector spacing (spatial resolution) of approximately 3.7 mm × 3.7 mm. The median filter of Davis 7.2 software was utilized to remove the spurious velocity vectors during the vector postprocessing, which limited the values of particle velocities (u) in the range of $u_{avg} \pm 3u_{RMS}$, where u_{avg} is the average value of eight neighbor vectors and u_{RMS} is the root-mean-square value of eight neighbor vectors. Such a reliable method for identifying spurious vectors is available even when certain spurious vectors are present (LaVision Gmbh, 2009). For each PIV test, 300 image pairs were acquired at the sampling frequency of 4.5 Hz (i.e., 66.67 s recordings).

In the past few decades, various vortex identification methods, including closed or spiraling streamlines (Lugt, 1979), pressure minima (Hunt et al., 1988), vorticity threshold (Hussain and Hayakawa, 1987; Bisset et al., 1990), etc., have been applied to interpret the vortical structures in the instantaneous flow fields. It should be noted that the existing methods for vortex identification may fail in certain scenarios due to their limitations. For example, the vorticity threshold method cannot discriminate between a vertical region with a swirl (when considered as a vortex) and a pure shear flow (not considered as a vortex).

In the present investigation, the swirling strength criterion is applied to quantify the intensity of the wake vortex shedding from the circular cylinder, i.e., the imaginary parts of the complex eigenvalues of the velocity gradient tensor were used to visualize the vortices. The velocity gradient tensor in two-dimensional Cartesian coordinates can be denoted as

$$\nabla \vec{u} = \begin{bmatrix} \frac{\partial u}{\partial x} & \frac{\partial u}{\partial y} \\ \frac{\partial v}{\partial x} & \frac{\partial v}{\partial y} \end{bmatrix} \tag{6}$$

The discriminant of the characteristic equation for velocity gradient tensor is given by

$$\Delta = \left(\frac{\partial u}{\partial x} + \frac{\partial v}{\partial y}\right)^2 - 4\left(\frac{\partial u}{\partial x}\frac{\partial v}{\partial y} - \frac{\partial u}{\partial y}\frac{\partial v}{\partial x}\right) \tag{7}$$

The velocity gradient tensor $\nabla \vec{u}$ may have two real eigenvalues ($\Delta \geq 0$) or a complex conjugate pair of complex eigenvalues ($\Delta < 0$) dependent on the value of the discriminant Δ. According to phase-plane theory, the streamlines exhibit a roughly circular or spiral pattern if two of the eigenvalues form a complex conjugate pair, which is consistent with the definition of vortex proposed by Robinson (1991). Chong et al. (1990) suggested the vortex core is a region of space where the velocity gradient tensor $\nabla \vec{u}$ has complex eigenvalues $\lambda_{cr} \pm \lambda_{ci}$i. Based on Zhou et al. (1999), the swirling strength λ_{ci} (i.e., the imaginary part of complex eigenvalues for the velocity gradient tensor) can be taken as an effective vortex indicator, and the region of $\lambda_{ci} > 0$ will be considered as vortices.

Table 1
Test conditions for ADV and PIV measurements.

Test No.	D (m)	u_e (m/s)	Re	e/D
A-1	0.04	0.06	2.34×10^3	2.0
A-2		0.11	2.86×10^3–3.50×10^3	0.10–2.0
A-3		0.22	7.67×10^3	2.0
A-4		0.32	1.13×10^4	2.0
A-5		0.42	1.49×10^4	2.0
B-1	0.08	0.06	4.45×10^3	2.0
B-2		0.11	6.30×10^3–7.72×10^3	0.10–2.0
B-3		0.22	1.54×10^4	2.0
B-4		0.32	2.24×10^4	2.0
B-5		0.42	2.92×10^4	2.0
C-1	0.12	0.06	7.03×10^3	2.0
C-2		0.11	1.00×10^4–1.23×10^4	0.10–2.0
C-3		0.22	2.30×10^4	2.0
C-4		0.32	3.38×10^4	2.0
C-5		0.42	4.47×10^4	2.0

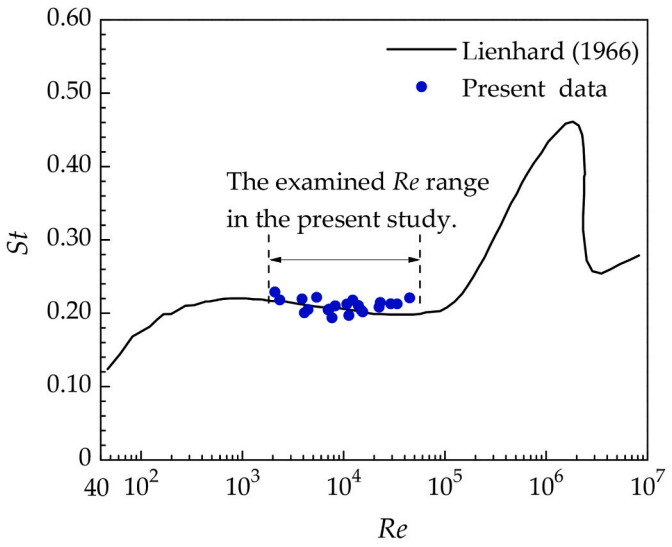

Fig. 6. Variation of *St* with *Re* for a smooth cylinder under the wall-free condition (Lienhard, 1966) and the examined *Re* range in the present study.

Among the existing methods for vortex identification, the swirling strength criterion has been proven to be much efficient for wall turbulence (Herpin et al., 2010). Thus, this vortex extraction method is adopted in the present PIV measurements. The swirling strength is defined as (see LaVision Gmbh, 2009):

$$\Omega = \max\left(0, -\frac{\Delta}{4}\right) \tag{8}$$

Note that the value of swirling strength (Ω) is equal to the square of λ_{ci}. The unit of swirling strength Ω is s^{-2}, and the value of Ω is proportional to the square of the frequency for a water particle swirling once (Chen et al., 2015).

2.2.3. Test conditions

Test conditions for ADV experiments are summarized in Table 1. To examine the scale effects, three plexiglass circular cylinders ($L = 1.0$ m) were employed, i.e., the outer diameter $D = 0.04$ m, 0.08 m and 0.12 m, respectively. The aspect ratio L/D of the cylinder falls between 8.3–25.0. The gap ratio (e/D) was varied by adjusting the vertical height of the cylinders. The values of e/D were set as 0.10, 0.20, 0.30, 0.40, 0.60, 0.80, 1.0, 1.5 and 2.0, respectively. And the far-field velocity at the water surface u_e was varied from 0.06 m/s to 0.42 m/s. Note: the PIV visualizations were merely carried out in the test A-2.

Fig. 6 shows the variation of *St* with *Re* for a wall-free smooth circular cylinder, in which the present experimental data for $e/D = 2.0$ are marked. As indicated in Fig. 6, the experimental data coincide well with the curve by Lienhard (1966). Moreover, the values of the *Re* in the present tests are in the range of 2.34×10^3–4.47×10^4, thus the flows are in the subcritical flow regime (i.e., $300 < Re < 3.0 \times 10^5$). The relationship between *St* and *Re* can be described by Roshko (1953) with an empirical formula (i.e., $St = 0.212–2.7/Re$) for the range of $3.0 \times 10^2 < Re < 2.0 \times 10^3$. Sarpkaya (2010) advised that such empirical formula can be used for the subcritical flow region. Hence, the effects of the Reynolds number on the vortex shedding frequency are negligible in the examined *Re* range. Nevertheless, under the condition of higher Reynolds numbers (e.g., $Re > 10^5$), *St* is significantly influenced by *Re* (see Fig. 6). It should be mentioned that the vortex shedding process of the cylinder is also affected by additional factors, e.g., the turbulence of the

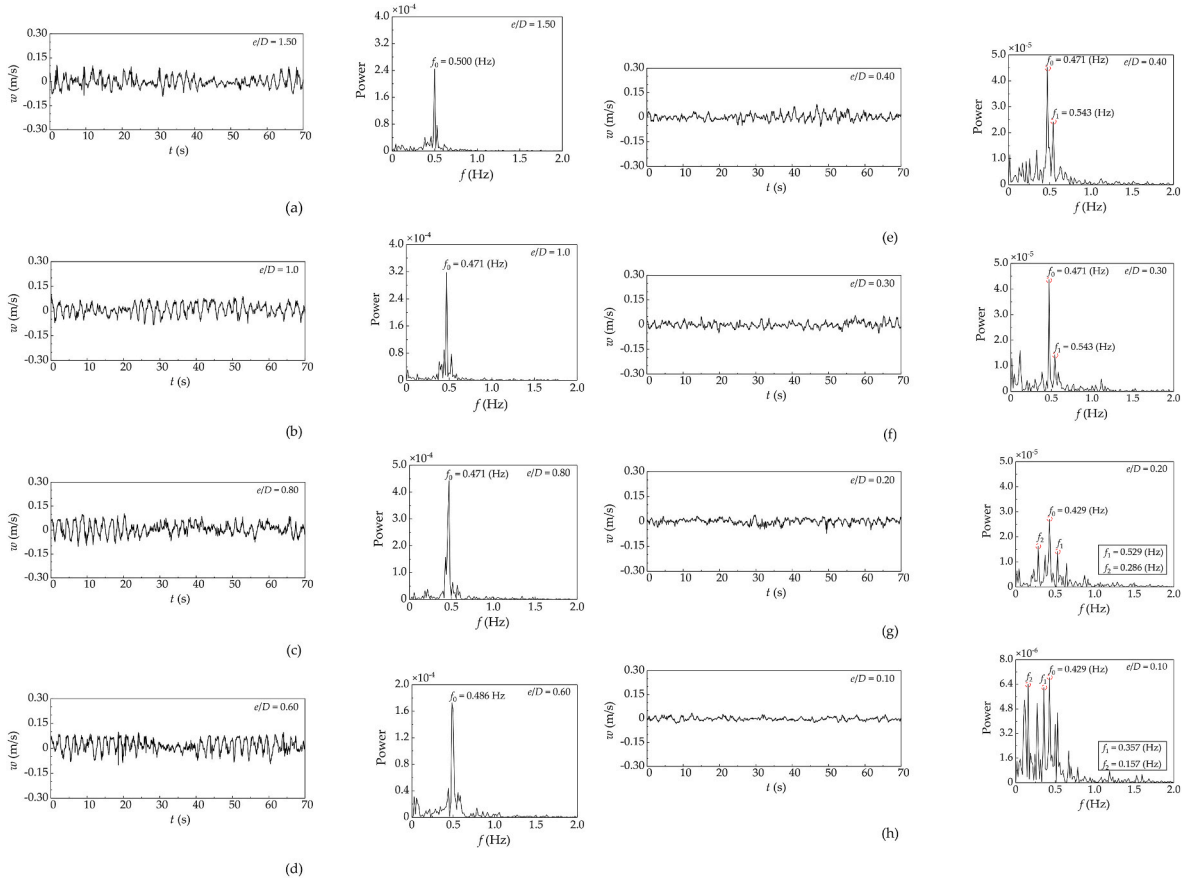

Fig. 7. Time histories of wake velocity (left column) and the corresponding power spectra (right column) for various values of e/D: (a) $e/D = 1.50$; (b) $e/D = 1.0$; (c) $e/D = 0.80$; (d) $e/D = 0.60$; (e) $e/D = 0.40$; (f) $e/D = 0.30$; (g) $e/D = 0.20$; (h) $e/D = 0.10$ (Test A-2: $D = 0.04$ m; $u_e = 0.11$ m/s).

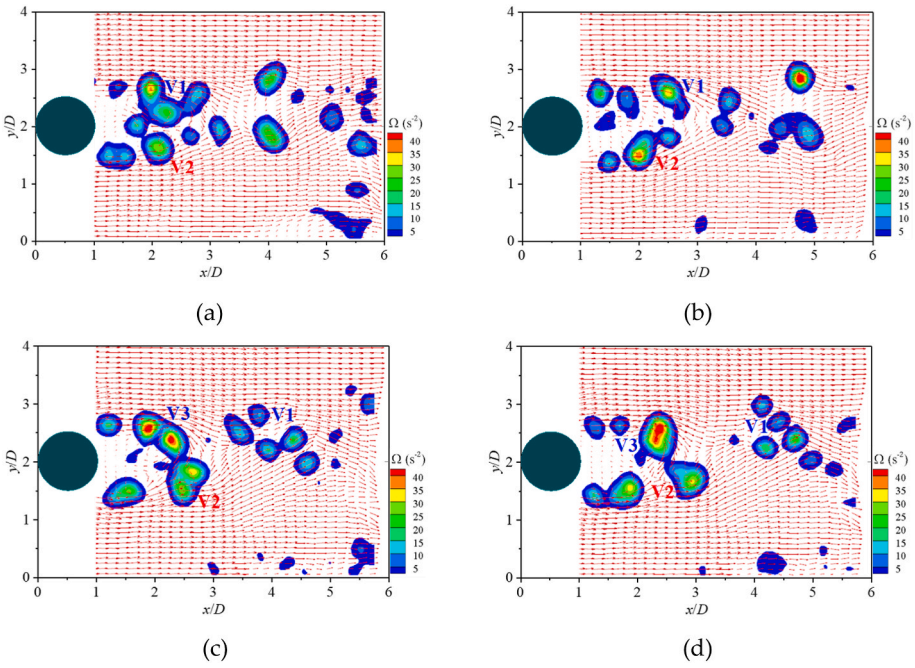

Fig. 8. Instantaneous velocity fields superposed with swirling strengths under the wall-free condition: (a) $t = 0$; (b) $t = T/4$; (c) $t = T/2$; (d) $t = 3T/4$ (Test A-2: $e/D = 1.50$; $Re = 3.39 \times 10^3$; $D = 0.04$ m).

incoming flow, and the roughness of the cylinder surface (Sumer, 2006).

3. Results and discussions

3.1. Multi-peaks for the lee-wake frequency of a near-wall cylinder

Based on Fast Fourier Transform (FFT), spectral analysis is made to investigate the periodic shedding characteristics. Fig. 7(a)-(h) show the time histories of the transverse velocities w (left column) and their corresponding power spectra (right column) for various values of e/D (Test A-2). Note that the transverse velocities (w) were measured by "ADV-2" at $x/D = 2.0$ and $y/D = e/D + 0.50$ (see Fig. 2).

Certain high frequency fluctuations appeared on the ADV records for time histories of the turbulent wake (see the left column of Fig. 7), but the dominant frequency $f_0 \approx 0.47 \pm 0.04$ Hz can be well identified in the frequency spectra for the lee-wake (see the right column of Fig. 7). Similar observations were made by Wang and Tan (2008) for $e/D = 0.20$–0.80. In the examined turbulent boundary layers, it was found that both the streamwise and the vertical turbulence intensities are generally in the range of 5%–12%, and the former gets larger than the latter especially while approaching to the bottom wall (Liu and Gao, 2022). Compared with the results for wall-free condition (e.g., $e/D \geq 1.50$, see Fig. 7(a)), the spectral peaks become relatively weaker while the cylinder getting closer to the wall, especially for $e/D \leq 0.40$ (see Fig. 7 (e)–(h)). Nevertheless, the spectrum can present remarkable peaks of the lee-wake frequency even at $e/D = 0.10$, indicating the periodicity of the wake still exists. Such multi-peaks phenomenon can be identified in the spectra of the lee-wake frequency for $e/D = 0.40$, 0.30, 0.20 and 0.10 (see Fig. 7(e)–(h)). Therefore, only using dominant-frequency would be not sufficient to describe the lee-wake characteristics for a near-wall cylinder. The multi-peaks spectra for the wake velocity around the cylinder have also been observed by previous researchers (see Lei et al., 1999; Price et al., 2002; Lin et al., 2009; He et al., 2017; Ouro et al., 2019; Zhou et al., 2021; Nguyen and Lei, 2021; Liu and Gao, 2022).

To describe the multi-peaks feature for the lee-wake, the discernible frequencies whose spectral power are larger than one-third of that for the dominant frequency would be taken into account. For $e/D = 0.40$ (see Fig. 7(e)), the dominant frequency (primary peak) is $f_0 = 0.471$ Hz,

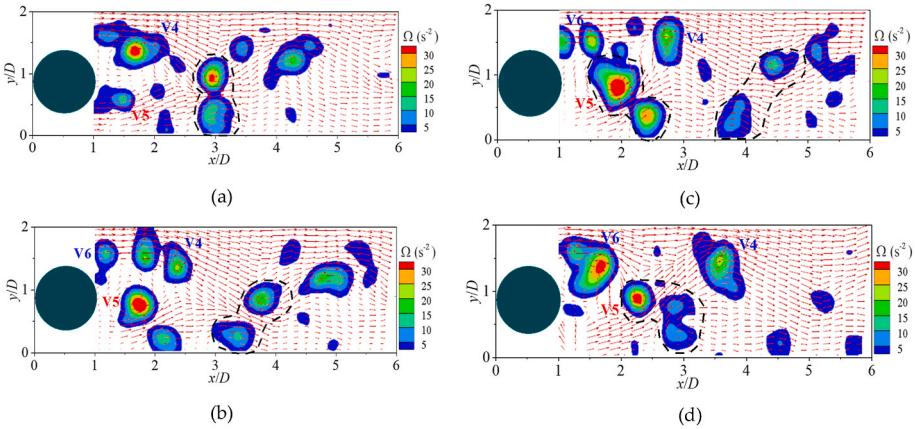

Fig. 9. Instantaneous velocity fields superposed with swirling strengths under the near-wall condition: (a) $t = 0$; (b) $t = T/4$; (c) $t = T/2$; (d) $t = 3T/4$ (Test A-2: $e/D = 0.40$; $Re = 3.02 \times 10^3$; $D = 0.04$ m).

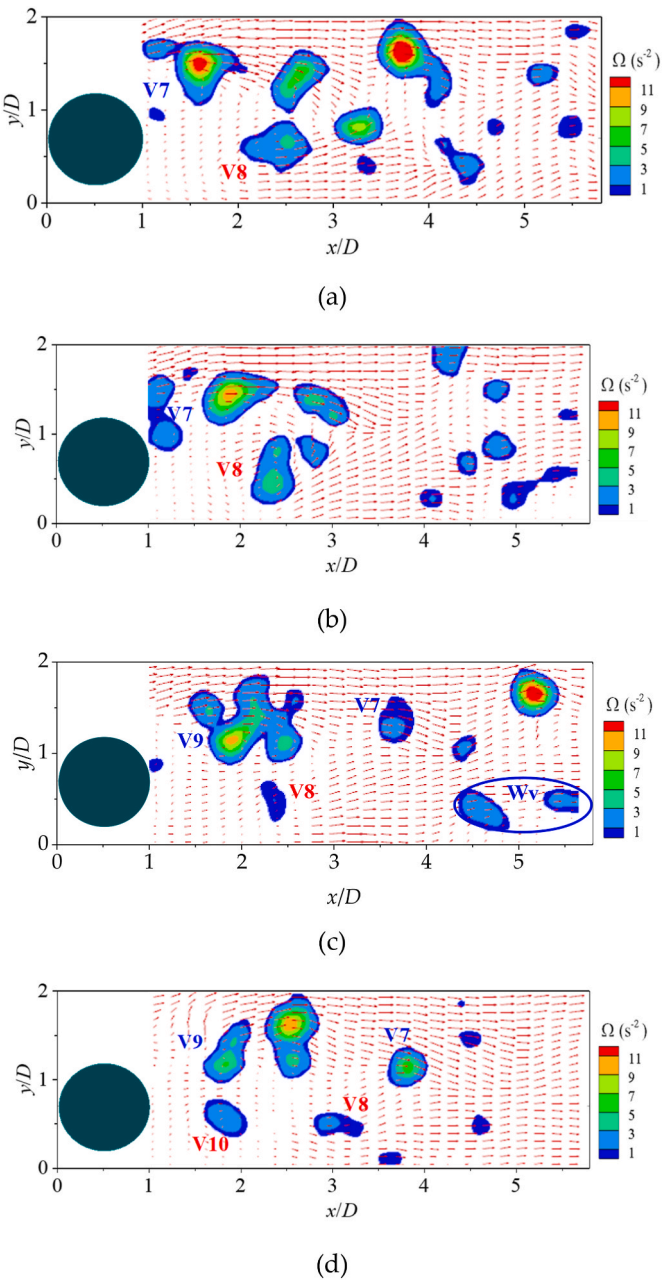

Fig. 10. Instantaneous velocity fields superposed with swirling strengths under the near-wall condition: (a) $t = 0$; (b) $t = T/4$; (c) $t = T/2$; (d) $t = 3T/4$ (Test A-2: $e/D = 0.20$; $Re = 2.91 \times 10^3$; $D = 0.04$ m).

and the secondary peak at $f_1 = 0.543$ Hz. For $e/D = 0.30$ (Fig. 7(f)), the dominant frequency is also $f_0 = 0.471$ Hz, and the secondary peak at $f_1 = 0.543$ Hz but with much weaker spectral power than that for $e/D = 0.40$. For $e/D = 0.20$ (Fig. 7(g)), the dominant frequency is $f_0 = 0.429$ Hz; however, there exists a secondary peak at $f_1 = 0.286$ Hz and an additional peak at $f_2 = 0.529$ Hz. Moreover, the dominant peak $f_0 = 0.429$ Hz for $e/D = 0.20$ is again captured for $e/D = 0.10$ (see Fig. 7(h)), indicating the possible similarity of shedding pattern for small values of e/D.

To better understand the aforementioned spectral characteristics featured with multi-peaks, PIV visualizations were further conducted for various values of e/D, i.e., $e/D = 1.5$, 0.4, and 0.2, respectively.

Fig. 8 shows the PIV measurements for a sequence of instantaneous velocity fields during a full period (T) under the wall-free ($e/D = 1.5$) and subcritical flow conditions, on which the swirling strengths are superposed. It was observed that the vortices were being shed alternatively from the upside (top) and the downside (bottom) of the circular cylinder. At $t = 0$ (see Fig. 8(a)), a negative vortex (V1) was ever shed from the top of the circular, and a positive vortex (V2) was subsequently formed from the bottom. At $t = T/4$ (Fig. 8(b)), the vortices V1 and V2 began moving downstream. A neonatal vortex V3 was then formed from the top of the cylinder ($t = T/2$, Fig. 8(c) and began moving downstream ($t = 3T/4$, Fig. 8(d)). A single frequency peak would be clearly detected in the spectrum for the regular vortex shedding under the wall-free condition (see Fig. 7(a)). As well known, such Kármán-like vortices are periodically shed from the wall-free cylinder with a certain frequency following the Strouhal law.

Similarly, the instantaneous flow velocity fields superposed with swirling strengths at $e/D = 0.40$ are shown in Fig. 9. Although the swirling strengths of the lee-wake get somewhat weaker than those for $e/D = 1.50$ (see Fig. 8), Kármán-like vortex shedding can still be identified by the PIV visualizations. It was observed that the evolution of vortices V4 ~ V6 (Fig. 9) is parallel to the vortices V1 ~ V3 (Fig. 8). Both shear layers were shed from the top and the bottom of the cylinder and curled up alternatively, producing a regular vortex shedding pattern. It should be mentioned that, for $e/D = 0.40$, the Kármán vortex-Wall vortex (Kv-Wv) interaction was observed, which is marked with black dashed lines in Fig. 9. Such Kv-Wv interaction phenomenon was also observed by other researchers (e.g., Ouro et al. (2019); Nguyen and Lei (2021)). As shown in Fig. 9, the wall vortex presented a clockwise rotation, while the Kármán vortex developed from bottom of the cylinder presented an anti-clockwise one. Once the Kármán vortex and the underlying wall vortex interacted with each other, the lee-wake would break into a few discrete vortices. The Kv-Wv interactions may lead to the multi-peaks phenomenon of the power spectrum, as shown in Fig. 7 (e).

As the cylinder gets further closer to the wall (e.g., $e/D = 0.20$, see Fig. 10), the evolution of instantaneous flow fields was also visualized with the upward-illumination PIV system. From the vortices V7 and V9 in Fig. 10(a)–(d), one can recognize that the upper shear layer flow shed from the top of the cylinder was still periodic. Meanwhile, the vortex V8 was being shed from the bottom of the cylinder. Nevertheless, the traveling velocity of V8 was much slower than that of V7 and V9. It took the vortex V8 about $3T/4$ (from $t = 0$–$3T/4$) to move from the position $x/D = 2.5$ to 3.0; while during this period, the vortex V7 originated from the upper shear layer has moved from $x/D = 1.5$ to 4.0 (see Fig. 10(a)–(d)). As shown in Fig. 10(b) and (c), the vortex in the lower shear layer seemed to be frozen, i.e., no alternative shedding vortex was developed therein. Although the lower shear layer exhibited an upward deflection, the wall vortices (Wv, marked by blue circles in Fig. 10(c)) were not strong enough to shed into several discrete vortices. Such phenomenon was ever explained as that the concentrated vorticity from the bottom of the cylinder was canceled by the opposite vorticity along the wall for small values of e/D (Grass et al., 1984; Taniguchi and Miyakoshi, 1990). Under the condition of small e/D (e.g., $e/D = 0.10$, and 0.20), the strength of vortices became weaker owing to intense Kv-Wv interactions. The multi-peaks in the spectra could be attributed to the difference in celerity between the lower wake vortex and the upper wake vortex, which is consistent with the observation of Sarkar and Sarkar (2010) in their numerical investigation.

3.2. Scale effects on the lee-wake characteristics

According to Eq. (5), the shear parameter (K) is mainly dependent on the gap ratio (e/D) for a cylinder in the bottom shear flow. It can be noticed that, for the same value of e/D, the cylinder with a smaller diameter would be closer to the bed. As such, the boundary influence could be more significant for the smaller cylinder, and the corresponding velocity fluctuations in the lee-wake could be different. As aforementioned, three series of flume tests for larger diameter of the cylinder (i.e., $D = 0.04$ m, 0.08 m, and 0.12 m, see Table 1) were conducted to

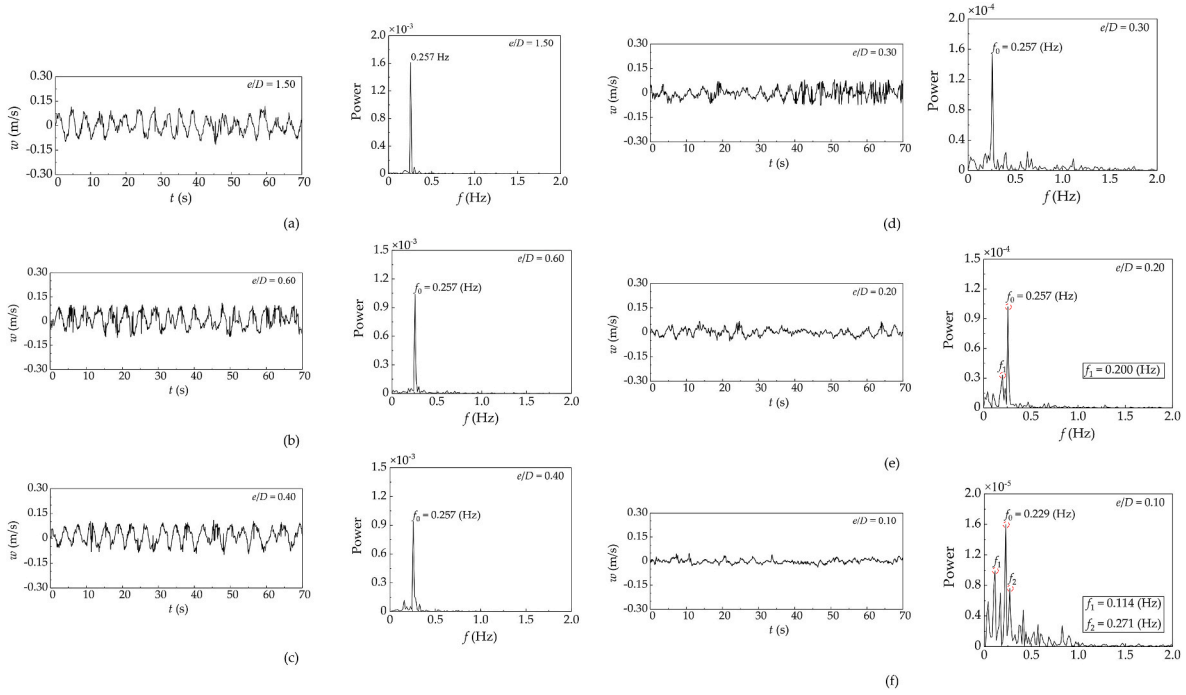

Fig. 11. Time histories of wake velocity (left column) and the corresponding power spectra (right column) for various values of e/D: (a) $e/D = 1.50$; (b) $e/D = 0.60$; (c) $e/D = 0.40$; (d) $e/D = 0.30$; (e) $e/D = 0.20$; (f) $e/D = 0.10$ (Test B-2: $D = 0.08$ m; $u_e = 0.11$ m/s).

examine the scale effects on the lee-wake characteristics.

The time histories of the transverse velocities (w) and the corresponding power spectra at various gap ratios (e/D) for $D = 0.08$ m and 0.12 m are shown in Figs. 11 and 12, respectively. Note that the results for $D = 0.04$ m are given in Fig. 7.

As shown in Fig. 11, the same dominant-frequency ($f_0 = 0.257$ Hz) was detected for all values of e/D (certain deviation for $e/D = 0.10$, see Fig. 11(f)), indicating periodic fluctuations were predominant in the lee-wake of the bigger cylinder ($D = 0.08$ m). No additional shedding frequency was measured under the condition $e/D = 0.40$ for $D = 0.08$ m (see Fig. 11(c)), which is different from the multi-peaks phenomenon for the smaller cylinder with $D = 0.04$ m (see Fig. 7(e)). The multi-peaks phenomenon was observed for $e/D \leq 0.20$ (see Fig. 11(e)–(f)), but the number of additional frequencies is reduced in comparison with Fig. 7 (f)–(g). For $e/D = 0.20$ (see Fig. 11(e)), the dominant-frequency is $f_0 = 0.257$ Hz and the secondary peak is at $f_1 = 0.200$ Hz. But for $e/D = 0.10$ (see Fig. 11(f)), besides the dominant-frequency $f_0 = 0.229$ Hz, there exist a secondary peak at $f_1 = 0.114$ Hz and another peak at $f_2 = 0.271$ Hz.

Similar to the results for $D = 0.08$ m (see Fig. 11), an exactly same dominant-frequency $f_0 = 0.186$ Hz was identified for all cylinders with $D = 0.12$ m in their spectra for different e/D in Fig. 12(a)–(f). The multi-peaks phenomenon was still detected in the spectrum for $e/D = 0.10$ (see Fig. 12(f)): i.e., $f_0 = 0.186$ Hz, and $f_1 = 0.071$ Hz.

Under the same conditions of u_e and e/D, the comparisons of spectral features for different values of D (see Figs. 7, 11 and 12) indicate that the multi-peaks response tends to get more remarkable with decreasing D. In other words, the wake fluctuations would get more regular for a larger cylinder. For the examined cylinders with various diameters, the critical gap ratios for multi-peaks spectra are $e/D \leq 0.40$ (for $D = 0.04$ m, see Fig. 7), $e/D \leq 0.20$ (for $D = 0.08$ m, see Fig. 11), and $e/D \leq 0.10$ (for $D = 0.12$ m, see Fig. 12), respectively. Note that such observations regarding multi-peak spectra were made under the subcritical flow conditions, and the corresponding gap-to-boundary layer thickness ratios $e/\delta \leq 0.032$. The variations of St with K for different values of D will be discussed in Section 3.3.

3.3. Bed-proximity effects on Strouhal number

As aforementioned in Section 2.2.1, the shear parameter (K) is a dimensionless parameter for characterizing the shear effect of approaching flow, which can be correlated with the gap ratio (e/D) (see Eq. (5)). As such, the shear parameter (K) can be used to evaluate the effects of bed proximity on the Strouhal number (St).

Based on the present flume observations (see Sections 3.1 and 3.2), the variations of the Strouhal number (St) with the shear parameter (K) for the condition of $u_e = 0.11$ m/s are given in Fig. 13. Note that the dominant shedding frequencies (f_0) are employed to calculate the Strouhal number. As shown in Fig. 13, the variations of the Strouhal number with K nearly kept the same trend for different diameters, the values of St increase gradually with the increase of shear parameter K. While the cylinder approaches the bed, the interactions between the shear layer separated behind the circular cylinder and the wall boundary layer would be much more complex. As indicated by the spectrum analyses of the wake velocity, the multi-peak phenomenon was observed for $e/\delta \leq 0.032$ (see Fig. 7(e)–(h), Fig. 11(e)–(f), Fig. 12(f), which may further bring the significant dispersion for larger K (see Fig. 13).

The Strouhal numbers measured in the present tests as well as those reported in the previous investigations are summarized in Fig. 14(a). It should be noticed that all the researchers (except for Grass et al. (1984), Lei et al. (1999), and Liu and Gao (2022)) conducted their experiments in the linear shear flow, which differs from the boundary shear flow in this study. By fitting these experimental data based on the least square method, the following empirical formula can be established to quantify the variation of St with K:

$$St = 0.25 - 0.06\tanh(0.08 / K - 0.24) \ (\text{for } 0 < K \leq 0.26) \tag{9}$$

Note that the present flume results were obtained under the range of gap ratios $0.10 \leq e/D \leq 2.0$ conditions (correspondingly, $0.06 \leq K \leq 0.24$), while Eq. (9) is established based on the present results of flume tests and previous results by other researchers.

As shown in Fig. 14(a), the variation of St with K agrees well with the predictions of Eq. (9). In general, the Strouhal number is approximately kept constant for $K < 0.04$, then the values of St increase gradually from

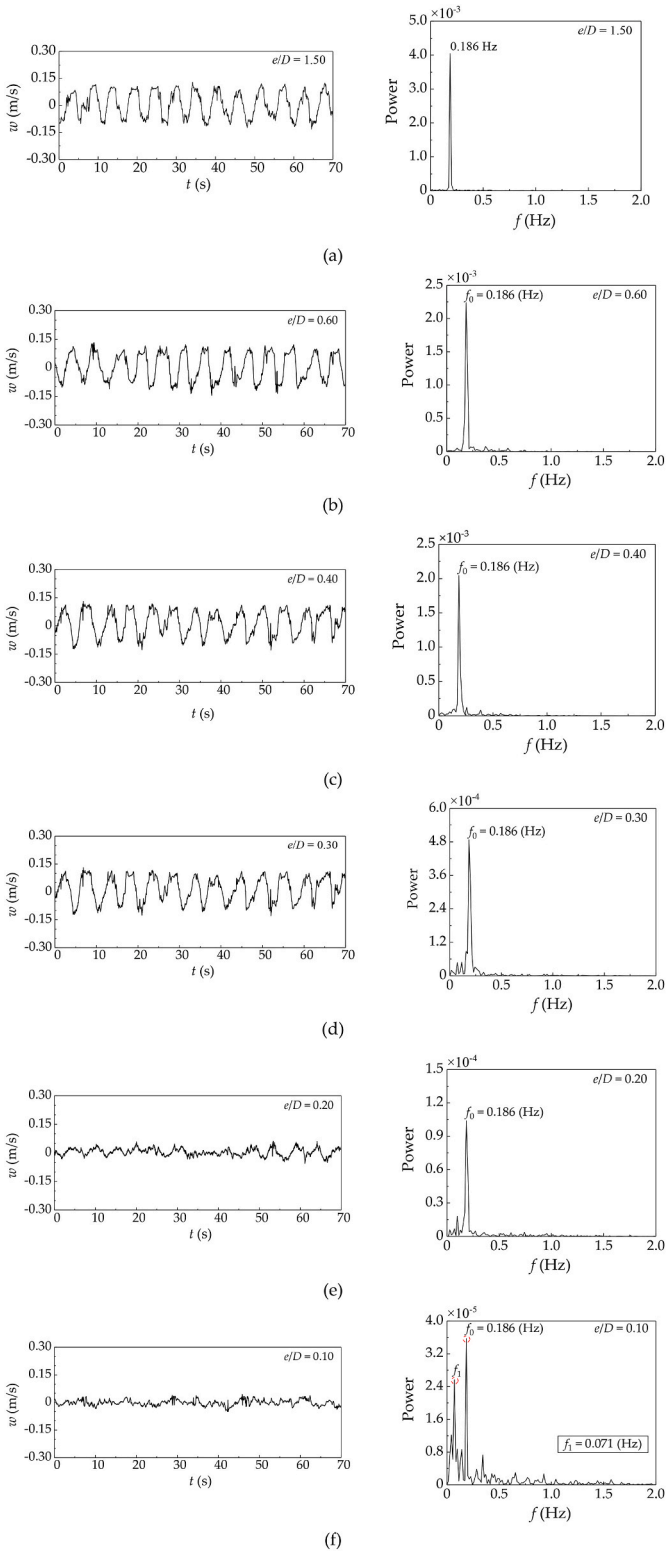

Fig. 12. Time histories of wake velocity (left column) and the corresponding power spectra (right column) for various values of e/D: (a) $e/D = 1.50$; (b) $e/D = 0.60$; (c) $e/D = 0.40$; (d) $e/D = 0.30$; (e) $e/D = 0.20$; (f) $e/D = 0.10$ (Test C-2: $D = 0.12$ m; $u_e = 0.11$ m/s).

0.193 up to around 0.246 with the increase of K from 0.04 to 0.26 (the corresponding e/D from about 3.0 to 0.05). Fig. 14(b) shows the comparison between the experimental (measured) data and the predicted values of St with Eq. (9), indicating that they are within the range of the

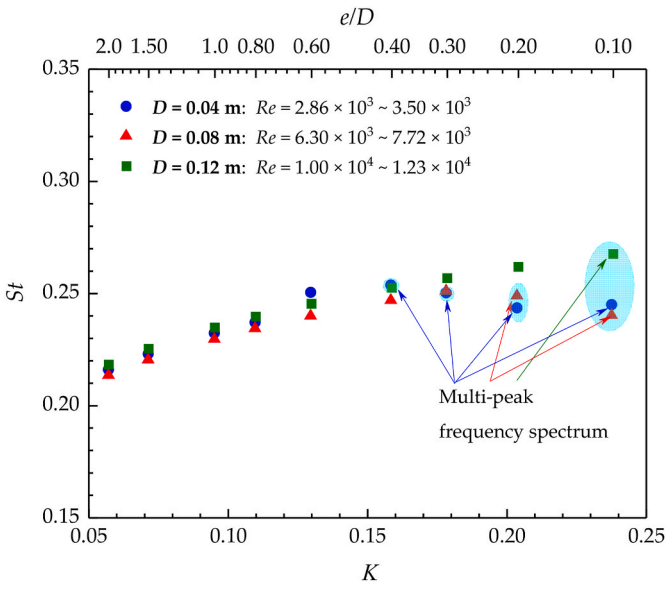

Fig. 13. Variations of St with K for different values of D ($D = 0.04$ m, 0.08 m, 0.12 m).

15% error lines. The deviations between these experimental data could be attributed to the difference in the Reynolds numbers (Re) and approach flow conditions such as the thickness of the boundary layer.

As aforementioned in Section 2.2.1, the relationship between the non-dimensional shear parameter (K) and the gap ratio (e/D) can be explicitly expressed with Eq. (5). Substituting Eq. (5) into Eq. (9), one can further derive the relationship between St and e/D:

$$St = 0.25 - 0.06\tanh(0.56\, e/D + 0.04) \ (\text{for } 0.10 \le e/D \le 2.0) \tag{10}$$

which may provide a reference for evaluating the lee-wake fluctuations of a free-spanning pipeline.

4. Conclusions

The bed-proximity effects on the vortex shedding frequency (or Strouhal number) of flow past a cylinder in the subcritical flow regime were investigated experimentally. The velocity fluctuations of lee-wake were measured with an Acoustic Doppler Velocimeter (ADV) and interpreted with power spectral analysis; meanwhile, the visualizations of wake flow behind the cylinder were conducted with an upward-illumination PIV system. Based on the dimensional analyses and flume observations, the following conclusions can be drawn:

(1) The shear parameter (K) is introduced to examine the bed-proximity effects on the Strouhal number for a circular cylinder in a boundary shear flow in the subcritical flow regime, and an explicit expression for the relationship between K and e/D is derived based on the boundary layer theory and verified with experimental data for a circular cylinder fully immersed in the turbulent boundary layer.

(2) The wake velocity fluctuations and the corresponding power spectra for the cylinders with three typical diameters were carefully examined by the ADV measurements. The variation trends of the Strouhal number with K were kept unchanged for different cylinder diameters. However, the values of e/D to cause the appearance of the multi-peak spectrum were related to the cylinder diameters. The PIV measurements indicate that the emergence of multi-peak spectra may be attributed to the significant interactions between the lower shear layer and the wall boundary layer.

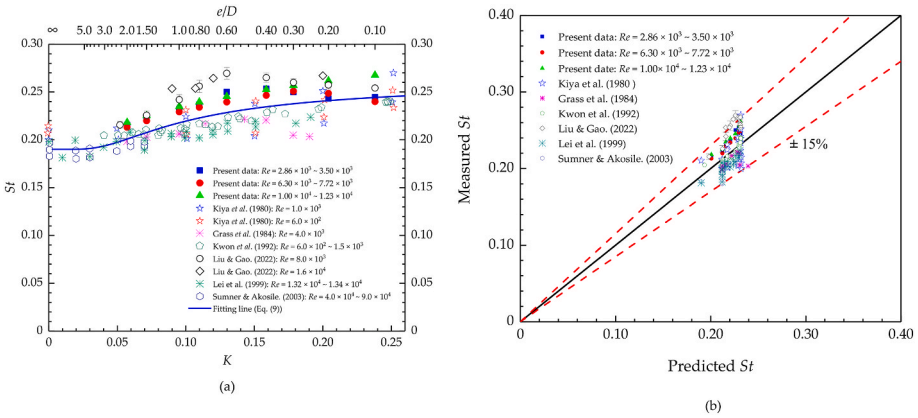

Fig. 14. (a) Variation of St with K for different Reynolds numbers (Re); (b) Comparison between the measured and the predicted values of St.

(3) Based on the present data and previous investigations, the empirical relationship between the Strouhal number (St) and K is established in the subcritical flow regime. Under the condition of $K < 0.04$, St seems to be independent of K and keeps almost constant, and then St increase with the increasing K for the case of $K > 0.04$. The maximum value of the Strouhal number (0.246) increased by approximately 30% more than that in the uniform flow condition (0.190).

It should be noted that the present study is predominantly limited to the sub-critical flow condition ($300 < Re < 3.0 \times 10^5$). Higher Reynolds numbers could be encountered in the fields. If the shear flow condition doesn't fall into the sub-critical region, certain deviations may exist when evaluating the Strouhal number with Eq. (10). The characterizations for the Strouhal number around a near-wall cylinder in the supercritical flow regime need to be further investigated.

CRediT authorship contribution statement

Yan Liu: Writing – original draft, preparation, Experiments, Formal analysis. **Jun Liu:** Validation, Formal analysis. **Fu-Ping Gao:** Conceptualization, Writing – review & editing, Supervision, All authors have read and agreed to the submitted version of the manuscript.

Declaration of competing interest

The authors declare that they have no known competing financial interests or personal relationships that could have appeared to influence the work reported in this paper.

Data availability

No data was used for the research described in the article.

Acknowledgments

This study was financially supported by the National Natural Science Foundation of China (Grant Nos. 11825205, 12061160463). Technical assistance from Mr. Fu-lin Zhang for the flume experiments is greatly appreciated.

Notation

D	Outer diameter of the cylinder
e	Gap between the cylinder bottom and the bed
f_s	Wake vortex shedding frequency
$f_{wall\text{-}free}$	Vortex shedding frequency for wall-free cylinder
f_0	Dominant shedding frequency
f_1, f_2	Other discernible shedding frequency
G	Transverse velocity gradient of the shear flow
h	Water depth
H_{dm}	Shape factor
K	Shear parameter
L	Spanwise length
n	Empirical parameter in Eq. (2)
Re	Reynolds number
St	Strouhal number
T	Vortex shedding period
u	Streamwise velocity along with the water depth
u_c	Approach velocity at cylinder center position
u_e	Approach Velocity at the water surface
u_l	Approach velocity at the level of the lower surface of the cylinder
u_u	Approach velocity at the level of the upper surface of the cylinder
u_{avg}	The average value of eight neighbor vectors
u_{RMS}	The root-mean-square value of eight neighbor vectors
x	Streamwise coordinate axis

y	Vertical coordinate axis
Δ	Discriminant defined in Eq. (7)
$\nabla\vec{u}$	Velocity gradient tensor
δ	Boundary layer thickness
δ_{d}	Displacement thickness of the boundary layer
δ_{m}	Momentum thickness of the boundary layer
λ_{ci}	Imaginary part of complex eigenvalues for the velocity gradient tensor
λ_{cr}	Real part of complex eigenvalues for the velocity gradient tensor
ρ	Mass density of fluid
ν	Kinematic viscosity of the fluid
Ω	Swirling strength

References

Adrian, R.J., Meinhart, C.D., Tomkins, C.D., 2000. Vortex organization in the outer region of the turbulent boundary layer. J. Fluid Mech. 422, 1–54. https://doi.org/10.1017/S0022112000001580.

Angrilli, F., Bergamaschi, S., Cossalter, V., 1982. Investigation of wall induced modifications to vortex shedding from a circular cylinder. J. Fluid Eng. 104 (4), 518–522. https://doi.org/10.1115/1.3241896.

Blevins, R.D., 1990. Flow-Induced Vibration. Krieger Publishing Company, California.

Bisset, D., Antonia, R.A., Browne, L.W.B., 1990. Spatial organization of large struct-ures in the turbulent far wake of a cylinder. J. Fluid Mech. 218, 439–461. https://doi.org/10.1017/S0022112090001069.

Bearman, P.W., Zdravkovich, M.M., 1978. Flow around a circular cylinder near a plane boundary. J. Fluid Mech. 89, 33–47. https://doi.org/10.1017/S0022112078002-44X.

Bhunia, A., Sikdar, P., Dash, S.M., Lua, K.B., 2019. Characterisation of Steady Flow Regime and Drag Force on the Forward and Backward Facing Trapezoidal Cylinders: a Numerical Study. Proceedings of 46th National Conference on Fluid Mechanics and Fluid Power, pp. 1–4.

Chen, Q.G., Zhong, Q., Qi, M.L., Wang, X.K., 2015. Comparison of vortex identification criteria for planar velocity fields in wall turbulence. Phys. Fluids 27. https://doi.org/10.1063/1.4927647, 0851-01.

Cao, S., Ozono, S., Hirano, K., Tamura, Y., 2007. Vortex shedding and aerodynamic forces on a circular cylinder in linear shear flow at subcritical Reynolds number. J. Fluid Struct. 23 (5), 703–714. https://doi.org/10.1016/j.jfluidstructs.2006.11.004.

Chong, M.S., Perry, A.E., Cantwell, B.J., 1990. A general classification of three-dimensional flow fields. Phys. Fluids 2 (5), 765–777. https://doi.org/10.1063/1.857730.

Dash, S.M., Lee, T.S., 2014. A novel flexible forcing hybrid ib-lbm scheme to simulate flow past circular cylinder. Int. J. Mod. Phys.: Conf. Ser. 25 (1), 1340014.

Dash, S.M., Triantafyllou, M.S., Alvarado, P.V.Y., 2020. A numerical study on the enhanced drag reduction and wake regime control of a square cylinder using dual splitter plates. Comput. Fluids 199, 1–13.

Fredsøe, J., Sumer, B.M., Andersen, J., Hansen, E.A., 1987. Transverse vibrations of a cylinder very close to a plane wall. J. Energy Resour. Technol. 109, 52–60. https://doi.org/10.1115/1.3256990.

Fredsøe, J., 2016. Pipeline-seabed interaction. J. Waterw. Port. Coast. 142 (6), 03116002 https://doi.org/10.1061/(ASCE)WW.1943-5460.0000352.

Grass, A., Raven, P.W.J., Stuart, R.J., Bray, J.A., 1984. The influence of boundary layer velocity gradients and bed proximity on vortex shedding from free spanning pipelines. J. Energy Resour. Technol. 106 (1), 70–78. https://doi.org/10.1115/1.3231028.

Gao, F.P., Gu, X.Y., Jeng, D.S., 2003. Physical modeling of untrenched submarine pipeline instability. Ocean Eng. 30 (10), 1283–1304. https://doi.org/10.1016/S0029-8018(02)00108-7.

Gao, F.P., Yang, B., Wu, Y.X., Yan, S.M., 2006. Steady currents induced seabed scour around a vibrating pipeline. Appl. Ocean Res. 28 (5), 291–298. https://doi.org/10.1016/j.apor.2007.01.004.

Gao, F.P., 2017. Flow-pipe-soil coupling mechanisms and predictions for submarine pipeline instability. J. Hydrodyn. 29 (5), 763–773. https://doi.org/10.1016/S1001-6058-(16)60787-4.

He, G.S., Wang, J.J., Pan, C., Feng, L.H., Gao, Q., Rinoshika, A., 2017. Vortex dynamics for flow over a circular cylinder in proximity to a wall. J. Fluid Mech. 812, 698–720. https://doi.org/10.1017/jfm.2016.812.

Herpin, S., Stanislas, M., Soria, J., 2010. The organization of near-wall turbulence: a comparison between boundary layer SPIV data and channel flow DNS data. J. Turbul. 11, 1–30. https://doi.org/10.1080/14685248.2010.508460.

Hunt, J.C.R., Wray, A.A., Moin, P., 1988. Eddies, Stream, and Convergence Zones in Turbulent Flows. Center for Turbulence Research Report CTR-S88, pp. 193–208.

Hussain, A.F., Hayakawa, M., 1987. Eduction of large-scale organized structures in a turbulent plane wake. J. Fluid Mech. 180, 193–229. https://doi.org/10.1017/S0022112087001782.

Kiya, M., Tamura, H., Arie, M., 1980. Vortex shedding from a circular cylinder in moderate-Reynolds-number shear flow. J. Fluid Mech. 101 (4), 721–735. https://doi.org/10.1017/S0022112080001899.

Kwon, T.S., Sung, H.J., Hyun, J.M., 1992. Experimental investigation of uniform-shear flow past a circular cylinder. J. Fluid Eng. 114, 457–460. https://doi.org/10.1115/1.2910053.

Lei, C., Cheng, L., Kavanagh, K., 1999. Re-examination of the effect of a plane boundary on force and vortex shedding of a circular cylinder. J. Wind Eng. Ind. Aerod. 80 (3), 263–286. https://doi.org/10.1016/S0167-6105(98)00204-9.

Lei, C.W., Cheng, L., Armfield, S.W., Kavanagh, K., 2000. Vortex-shedding suppression for flow over a circular cylinder near a plane boundary. Ocean Eng. 27, 1109–1127. https://doi.org/10.1016/S0029-8018(99)00033-5.

Lienhard, J.H., 1966. Synopsis of Lift, Drag, and Vortex Frequency Data for Rrigid Circular Cylinders. Technical Extension Service, Washington.

LaVision Gmbh, 2009. Product-Manual for Davis 7.2 Software. Göttingen, Germany.

Lin, W.J., Lin, C., Hsieh, S.C., Dey, S., 2009. Flow characteristics around a circular cylinder placed horizontally above a plane boundary. J. Eng. Mech. 135, 697–716. https://doi.org/10.1061/(ASCE)0733-9399(2009)135:7(697).

Liu, J., Gao, F.P., 2022. Triggering mechanics for transverse vibrations of a circular cylinder in a shear flow: wall-proximity effects. J. Fluid Struct. 108, 103423 https://doi.org/10.1016/j.jfluidstructs.2021.103423.

Lueck, R., Laurent, L.S., Moum, J., 2009. Turbulence in the Benthic Boundary Layer (Cambridge).

Lugt, H., 1979. The dilemma of defining a vortex. In: Recent Developments in Theoretical and Experimental Fluid Mechanics. Springer, Berlin.

Nguyen, Q.D., Lei, C.W., 2021. A particle image velocimetry measurement of flow over a highly confined circular cylinder at 60% blockage ratio. Phys. Fluids 33 (10), 104111. https://doi.org/10.1063/5.0066606.

Niemann, H.J., Holscher, N., 1990. A review of recent experiments on the flow past circular cylinders. J. Wind Eng. Ind. Aerod. 33 (1–2), 197–209. https://doi.org/10.1016/0167-6105(90)90035-B.

Ouro, P., Muhawenimana, V., Wilson, C.A.M.E., 2019. Asymmetric wake of a horizontal cylinder in close proximity to a solid boundary for Reynolds numbers in the subcritical turbulence regime. Phys. Rev. Fluids. 4, 104604 https://doi.org/10.1103/PhysRevFluids.4.104604.

Price, S., Sumner, D., Smith, J.G., Leong, K., Paidoussis, M.P., 2002. Flow visualization around a circular cylinder near to a plane wall. J. Fluid Struct. 16, 175–191. https://doi.org/10.1006/jfls.2001.0413.

Robinson, S.K., 1991. Coherent motions in the turbulent boundary layer. Annu. Rev. Fluid Mech. 23, 601–639. https://doi.org/10.1146/annurev.fl.23.010191.003125.

Roshko, A., 1953. On the Development of Turbulent Wakes from Vortex Streets. National Advisory Committee for Aeronautics, Washington.

Sarkar, S., Sarkar, S., 2010. Vortex dynamics of a cylinder wake in proximity to a wall. J. Fluid Struct. 26, 19–40. https://doi.org/10.1016/j.jfluidstructs.2009.08.003.

Stahr, F.R., Sanford, T.B., 1999. Transport and bottom boundary layer observations of the North Atlantic deep western boundary current at the Blake Outer Ridge. Deep-Sea Res. PT II 46, 205–243. https://doi.org/10.1016/S0967-0645(98)00101-5.

Sumer, B.M., 2006. Hydrodynamics Around Cylindrical Structures. World Scientific, Singapore.

Sarpkaya, T.S., 2010. Wave Forces on Offshore Structures. Cambridge University Press, Cambridge, UK.

Sumner, D., Akosile, O.O., 2003. On uniform planar shear flow around a circular cylinder at subcritical Reynolds number. J. Fluid Struct. 18 (3–4), 441–454. https://d-o-i.org/10.1016/j.jfluidstructs.2003.08.004.

Schlichting, H., 1979. Boundary-Layer Theory, seventh ed. McGraw-Hil, New York.

Taniguchi, S., Miyakoshi, K., 1990. Fluctuating fluid forces acting on a circular cylinder and interference with a plane wall. Exp. Fluid 9 (4), 197–204. https://doi.org/10.1007/bf00190418.

Wang, X., Tan, S.K., 2008. Near-wake flow characteristics of a circular cylinder close to a wall. J. Fluid Struct. 24 (5), 605–627. https://doi.org/10.1016/j.jfluidstructs.2-007.11.001.

Wang, X.K., Hao, Z., Tan, S.K., 2013. Vortex-Induced vibrations of a neutrally buoyant circular cylinder near a plane wall. J. Fluid Struct. 29, 188–204. https://doi.org/10.1016/j.jfluidstructs.2013.02.012.

Yang, B., Gao, F.P., Wu, Y.X., 2008. Flow-Induced vibrations of a cylinder with Two degrees of freedom near rigid plane boundary. Int. J. Offshore Polar Eng. 18 (4), 302–307. https://doi.org/10.1016/j.ijmecsci.2008.08.010.

Zdravkovich, M.M., 1997. Flow Around Circular Cylinders -Volume 1: Fundamentals. Oxford university press, London.

Zhou, J., Adrian, R.J., Balachandar, S., Kendall, T.M., 1999. Mechanisms for generating coherent packets of hairpin vortices in channel flow. J. Fluid Mech. 387, 353–396. https://doi.org/10.1017/S002211209900467X.

Zhou, J., Qiu, X., Li, J., Liu, Y., 2021. The gap ratio effects on vortex evolution behind a circular cylinder placed near a wall. Phys. Fluids 33 (3), 037112. https://doi.org/10.1063/5.0039611.